2019-02-11

Manipulation of subcortical and deep cortical activity in the primate brain using transcranial focused ultrasound stimulation

Folloni, D

10.1016/j.neuron.2019.01.019
Neuron
Elsevier

Manipulation of subcortical and deep cortical activity in the primate brain using transcranial focused ultrasound stimulation

Davide Folloni[1,2*†], Lennart Verhagen[1,2*†], Rogier B. Mars[2,3], Elsa Fouragnan[1,4], Charlotte Constans[5], Jean-François Aubry[5], Matthew F.S. Rushworth[1,2†], Jérôme Sallet[1,2*†]

[1]Wellcome Centre for Integrative Neuroimaging (WIN), Department of Experimental Psychology, University of Oxford, Oxford, UK

[2]Wellcome Centre for Integrative Neuroimaging (WIN), Centre for Functional MRI of the Brain (FMRIB), Nuffield Department of Clinical Neurosciences, John Radcliffe Hospital, University of Oxford

[3]Donders Institute for Brain, Cognition and Behaviour, Radboud University Nijmegen, Nijmegen, the Netherlands

[4]School of Psychology, University of Plymouth, UK

[5] Institut Langevin, ESPCI Paris, PSL Research University, CNRS 7587, UMRS 979 INSERM, Université Paris Diderot, Sorbonne Paris Cité, Paris, France.

†Authors contributed equally to the work

***To whom correspondence should be addressed:**

Address: **Davide Folloni, Lennart Verhagen, or Jerome Sallet**

Department of Experimental Psychology,

University of Oxford,

Tinsley Building,

Mansfield Road,

Oxford,

OX1 3SR, UK

E-mail:
davide.folloni@psy.ox.ac.uk
lennart.verhagen@psy.ox.ac.uk
jerome.sallet@psy.ox.ac.uk

Highlights

Ultrasound stimulation exerts regionally specific neural effects in primates

It can be used to alter activity even in subcortical and deep cortical areas

After stimulation activity in a brain area is less related to the rest of its network

The observed offline effects were not mediated by auditory artefact.

In Brief

Ultrasound can be used transcranially to modulate activity in deep brain areas. The effects are specific to the sonicated brain region, last for more than one hour and are not due to an auditory artefact.

Summary

The causal role of an area within a neural network can be determined by interfering with its activity and measuring the impact. Many current reversible manipulation techniques have limitations preventing their focal application particularly in deep areas of the primate brain. Here we demonstrate a transcranial focused ultrasound stimulation (TUS) protocol that manipulates activity even in deep brain areas: a subcortical brain structure, the amygdala (experiment 1), and a deep cortical region, anterior cingulate cortex (ACC, experiment 2), in macaques. TUS neuromodulatory effects were measured by examining relationships between activity in each area and the rest of the brain using functional magnetic resonance imaging (fMRI). In control conditions without sonication, activity in a given area is related to activity in interconnected regions but such relationships are reduced after sonication, specifically for the targeted areas. Dissociable and focal effects on neural activity could not be explained by auditory confounds.

INTRODUCTION

To establish the functional role of a brain area it is necessary to examine the impact of disrupting or altering its activity. It has recently been proposed that this might be accomplished with low-intensity transcranial focused ultrasound stimulation (TUS) (Tufail et al., 2011; King et al., 2013; Yoo et al., 2011). When used over the frontal eye field in macaques, TUS leads to latency change during voluntary saccades (Deffieux et al., 2013). Comparatively little, however, is known about TUS's impact on neural activity and if its effects persist after the stimulation has terminated. We show here that in the macaque (*Macaca mulatta*) TUS modulates neural activity and does so even in subcortical nuclei such as the amygdala and deep cortical regions such as anterior cingulate cortex (ACC). Moreover, we demonstrate a protocol that exerts an "offline" effect that lasts for an extended period of tens of minutes after an initial stimulation period of 40 s. This extended period of action is important because it means that its neural effect substantially outlasts any potential direct acoustic or somatosensory effects that might occur during the stimulation period itself (Guo et al., 2018; Sato et al., 2018). We also confirm this by showing that the stimulation protocol was not associated with any similarly sustained impact on the activity of the auditory system.

In addition we demonstrate that a considerable degree of focality is possible with TUS. The peak and extent of the TUS neuromodulatory effect closely matched those of the ultrasonic intensity as estimated by simulations of the acoustic wave propagation. When TUS is applied to amygdala its impact is most apparent in amygdala rather than in more distal regions or those between the stimulation cone and the target area. The same is true of ACC TUS; its impact is most apparent in ACC where the acoustic intensity is highest. The focal impact of offline TUS in deep brain structures may underlie the specific patterns of behavioral impairment recently reported when the same protocol was used in awake behaving animals (Fouragnan et al. BioRXiv).

RESULTS

Stimulation of deep brain structure and resting-state fMRI recording

On each session of TUS application, a 40 s train of pulsed ultrasound (250 kHz) comprising 30 ms bursts of ultrasound every 100 ms was directed to the target brain region using a single-element transducer in conjunction with a region-specific coupling cone filled with degassed water. To control for any confounds resulting from concomitant ultrasound stimulation and neural signal recording (Guo et al., 2018; Sato et al., 2018), recordings of neural activity only begun approximately 30 minutes after the end of TUS application when any potential auditory or somatosensory effects of stimulation were dissipated. We therefore refer to this stimulation protocol as an "offline" protocol.

Frameless stereotaxic neuronavigation was used to position the transducer over the target brain area taking into consideration the focal depth of the sonication (fig.1; experiment 1: amygdala n=4; experiment 2: ACC n=3; relatively deep brain regions known to be interconnected and co-active during similar cognitive processes such as social cognition (Munuera et al., 2018; Noonan et al., 2014). A single train was applied sequentially to each of the more laterally situated amygdalae, in experiment 1 and to the midline structure, ACC, in experiment 2.

The impact of TUS was determined by examining brain activity over an 80 minute period starting approximately 30 minutes after the 40 s stimulation train began (Supplementary Material). Activity was recorded not just from the stimulated site but from across the entire brain using functional MRI (fMRI). FMRI data from the stimulated animals was compared with data from an additional group of control individuals (n=9) that had received no TUS. Note that depth of anaesthesia and the delay between sedation induction and data acquisition were similar between the TUS and the control groups (0.7-0.8% and 0.7-1% range of expired isoflurane concentration, 1.53 and 2.38 hours, respectively; Supplementary Material). FMRI data were acquired at 3T under isoflurane anesthesia and preprocessed using established tools and protocols (Verhagen et al., BioRXiv; Supplementary Material). The anesthesia protocol has previously been shown to preserve regional functional connectivity measurable with fMRI (Sallet et al., 2013; Neubert et al., 2015).

Although the blood oxygen level dependent (BOLD) signal recorded with fMRI does not provide an absolute measure of activity it does provide a relative measure of activity change in relation to external events or activity recorded from other brain areas. This means that we cannot easily use BOLD to capture a measure such as activity in a brain area averaged over time. However, what we can do is to examine how BOLD responses in one area, such as the one that we are sonicating, relate to BOLD in another area using approaches similar to those employed previously (Sallet et al., 2013; Neubert et al., 2015; Vincent et al., 2007; Margulies et al., 2016; Margulies et al., 2009; Ghahremani et al., 2017; Mars et al., 2013; Shen, 2015; Shen et al., 2015; Hutchison et al., 2012).

Even at rest in the control state, BOLD activity in one area is correlated with BOLD activity in other areas and such relationships are most prominent when the areas are monosynaptically connected, although some residual connectivity is mediated by indirect connections (O'Reilly et al., 2013). The pattern of activity coupling for any given area reflects its unique constellation of projections and interactions, sometimes called its "connectivity fingerprint" (Passingham et al., 2002).

Focal effects of TUS on subcortical neural activity in the amygdala

To examine the spatial specificity of TUS effects and to investigate the capacity of TUS to stimulate subcortical structures we investigated its effects on the coupling of amygdala activity with activity in other brain areas.

Independently of the nature of the mechanisms underlying TUS (see Dallapiazza et al., 2018; Fomenko et al., 2018; Kubanek, 2018; Tyler et al., 2018), if amygdala TUS affects activity in amygdala in a specific manner then what we should see is that the normal relationship seen at rest between the activity in amygdala and activity elsewhere will change. This does not mean that activity induced by TUS is diffused across the brain or that it is induced in one area and then "spreads" to others. It means simply that the relationship between activity in one area and another is changing. Measurements of activity throughout any area of tissue that is similarly affected by the TUS may become more highly correlated with one another. However, if the stimulated tissue in the amygdala becomes less responsive to other inputs from elsewhere in the brain then the relationship between amygdala activity and elsewhere will decrease.

In the control state, the relationship between activity in amygdala and elsewhere suggests the amygdala is influenced by activity in other nodes of the network it is part of and *vice versa*. In controls, amygdala activity is coupled with activity in cingulate, ventral, and orbitofrontal cortex, striatum, and the anterior temporal lobe (figs. 2a,2g). In order to make a statistical comparison of the functional coupling of the amygdala in the control and amygdala TUS conditions it is problematic to compare coupling at each and every other point in the brain because there is a risk of false positive effects if multiple comparisons are made. Given the limited sample sizes possible with non-human primate experiments, however, there is a risk of false negative results if stringent correction for multiple comparisons is undertaken at the whole-brain level. Indeed, here we avoid these pitfalls and reproduce whole-brain functional connectivity maps unthresholded to report on the full extent of the effects. Importantly, statistical inference was drawn on a limited set of regions beyond the amygdala known to be interconnected with macaque amygdala from anatomical tracing studies (Amaral and Price, 1984) and to exhibit, again in macaques, activity coupling with the amygdala under anesthesia (Neubert et al., 2015). An additional consideration was that some of the areas were connected to (Van Hoesen et al., 1993) and exhibited activity coupling with (Neubert et al., 2015) ACC (the focus of the next experiment). Finally some areas, such as primary motor cortex (M1) and posterior intraparietal sulcus (pIPS) were chosen because, by contrast, they have limited connections and coupling with amygdala or ACC. The specific ROI locations were based on previous studies of resting state activity coupling in the macaque (Neubert et al., 2015; Neubert et al., 2014; Sallet et al., 2013). Rather than examining activity coupling between amygdala and each of these ROIs in turn (and risking potential false positive results), we compared the overall pattern or

"fingerprint" of coupling using the method devised by Mars and colleagues (Mars et al., 2016; Verhagen et al., BioRxiv); non-parametric permutation tests were performed on cosine similarity metrics summarizing pairs of fingerprints (amygdala TUS versus control).

The amygdala's activity coupling was significantly changed after amygdala TUS (non-parametric permutation test, p = 0.0020; figs. 2b,2g). A whole-brain quantitative analysis revealed that this effect of amygdala TUS was most apparent in the amygdala, and not anywhere else in the brain (fig.3a).

A second way to establish the specificity of TUS effects within the network is to examine whether the amygdala connectivity effects seen after amygdala TUS are found after ACC TUS. This was not the case; ACC TUS left most of amygdala's coupling pattern unaffected (non-parametric permutation test, p = 0.1346; figs.2c,2g) although not surprisingly ACC TUS led to alteration in amygdala's coupling with ACC.

Decrements in functional connectivity can reflect either a decrement in the coupling between otherwise stable neural signals, or a decrement in amplitude of the coupled neural signals (in the context of other signals and noise), or an increment in unstructured noise levels (Duff et al., 2018). When we examined the variance of the BOLD signal - a proxy for both the signal amplitude and the noise level - it was clear that there was little difference in the control state and after either amygdala or ACC TUS. This might suggest that TUS did not induce gross changes in signal amplitude or noise level, but rather more specific changes in signal coupling.

Finally, to further establish the nature of amygdala TUS effects within the network we investigated the activity coupling patterns of five further control areas. We investigated three regions adjacent to the amygdala and found their functional connectivity was unaltered (fig.3b). We also examined an area with a very distinct constellation of projections – ventral premotor area F5c – and again found no change (fig. S1). Similarly, below, we explain additional control analyses that confirmed that the TUS effect could not have been mediated via auditory cortex.

Focal effects of TUS on deep cortical neural activity in anterior cingulate cortex (ACC)

To examine the specificity of TUS effects further and to investigate the capacity of TUS to stimulate deep cortical structures we investigated the effects of ACC TUS on ACC activity. In control animals at rest ACC activity was coupled with activity in strongly connected areas: dorsal, lateral, and orbital prefrontal cortex (PFC), frontal pole, mid and posterior cingulate (figs. 2d,2h). After ACC TUS the ACC coupling pattern was altered (non-parametric permutation test, p = 0.0210; fig.2f,2h). A parsimonious interpretation is that normally the activity that arises in ACC is a function of the activity in the areas that project to it, but this is no longer the case when ACC's activity is artificially

driven or diminished by TUS. Because these interactions with other areas determine the information ACC receives from elsewhere in the brain and the influence it exerts over other areas, ACC TUS should alter ACC's computation and induce specific changes in behavior (Fouragnan et al., BioRXiv).

Similar to the analyses of spatial extent of amygdala TUS effects, we quantified the change in coupling induced by ACC TUS not only in ACC itself, but for every point in the brain. This analysis revealed that ACC TUS affected primarily the ACC.

The specificity and selectivity of the effects are further underscored by the results observed when mapping the coupling pattern of areas interconnected with the stimulated ACC region. First, we examined the activity coupling pattern of the amygdala – an area with which ACC is monosynaptically interconnected (Amaral and Price, 1984; Van Hoesen et al., 1993) and functionally coupled (Neubert et al., 2015). Not surprisingly, there was some evidence that amygdala-ACC coupling had changed as a function of ACC TUS, as had coupling with a third area – caudal orbitofrontal cortex – with which both ACC and amygdala are strongly interconnected. However, other aspects of the amygdala's coupling pattern were relatively unaltered by ACC TUS; although there was a trend in the non-parametric permutation test for amygdala connectivity to change after ACC TUS ($p = 0.0744$; figs. 2c,2h) it was clear that there was a significant difference between ACC and amygdala TUS effects (non-parametric permutation test, $p = 0.0428$).

Just as amygdala TUS did not affect the connectional profile of F5c, a region outside the interconnected network of the stimulated areas, ACC TUS also did not affect F5c's coupling (fig.S1). Again, below, we explain additional control analyses that confirmed that the TUS effect could not have been mediated via the auditory cortex.

The spatial and connectional specificity of the observed effects make it unlikely that the TUS induced modulations were mediated by general physiological effects, such as those related to anesthesia level and duration. Nonetheless, while the anesthesia levels as indexed by expired isoflurane concentrations were well matched between conditions (see Supplementary Materials), the delay between sedation and data collection was on average slightly longer in the control sessions (2.38h) than the amygdala TUS (2.00h; versus control: $F(1,34)=2.7654$, $p=0.10552$) and ACC TUS (1.44h; versus control: $F(1,31)=9.5537$, $p=0.0041946$). However, despite differences in the effects of ACC and amygdala TUS on functional connectivity, amygdala and ACC TUS sessions were very similar in duration ($F(1,19)=2.6863$, $p=0.11767$). Furthermore, there were no differences in any measurements of physiological parameters indexing the depth of anesthesia including expired isoflurane ($F(1.41)=0.37451$, $p=0.68995$), heart rate ($F(1,41)=1.8382$, $p=0.17198$), and respiration rate ($F(1,41)=0.032232$, $p=0.96831$) in control, amygdala, and ACC sessions. A final empirical

argument against the possibility that TUS effects were confounded with differences in duration under anesthesia at the time of scanning is that even though scanning occurred slightly later after the onset of anesthesia in the control sessions, the TUS effects on functional connectivity did not increase with time but, if anything slightly diminished with time; this was apparent when the resting state data were divided into three time bins (Supplementary Fig.S3).

Focality of TUS

Our major focus in the current investigation is primarily on the possibility of altering activity in deep brain structures with ultrasound and the sonication parameters adopted here have been optimized with this aim in mind (fig.1). In future experiments it will be possible to manipulate the ultrasound's features to enhance the spatial focality of any effects that we find, for example by sonicating at higher frequencies (500 kHz) and concomitant shorter wave lengths, or using multiple beams on different trajectories that intersect at the target location. Nevertheless, it is obviously of interest to examine the focality that is obtained with the current sonication parameters. Two additional sets of analyses were, therefore, also conducted. The first set of analyses assessed the impact of TUS not only for the target areas but for every point in the brain, while the second set focused in detail on the areas surrounding the target areas or located between the stimulation cone and the target area (figs.3, S2).

In the first set of analyses, for each point in the brain, we indexed its activity coupling with the same *a priori* defined constellation of regions used throughout the analyses (fig.2g,h), but now excluding the sonicated areas. We quantify the impact of TUS by comparing for each point the average coupling with this set of regions in the control condition with the coupling observed following amygdala TUS and following ACC TUS. This approach resulted in two 'heat-maps' that show the peak location and extent of the brain activity impacted by TUS over amygdala and ACC. Following amygdala TUS the strongest neuromodulatory effects were observed in the amygdala itself, and only in the amygdala (fig.3a, top row). Following ACC TUS the extent of the neuromodulation was limited to the ACC and regions immediately ventral to it along the ultrasound beam (fig.3a, bottom row). In fact, the spatial maps of TUS impact on activity coupling are strikingly in correspondence with the spatial maps of estimated sonication intensity (fig.1c,f). This correspondence is specific and sensitive: it includes particulars of the wave propagations, such as how the ultrasound wave targeted at amygdala reflects on the basal bone, while in the ACC TUS condition considerable acoustic energy is also deposited immediately ventral to the target along the trajectory, partly due to sound waves reflecting on the orbital bone.

To further qualify and examine the extent of the ultrasonic intervention, in the second set of analyses we measured activity coupling in a control state and after amygdala TUS in three control areas located along the trajectory of the ultrasound beam (fig.3b, sub-panels *ii* and *iii*) or just ventral to it (fig.3b, sub-panel *iv*). Confirming the whole-brain analyses of TUS impact and extent (fig.3a), there were no major changes in the activity coupling of areas situated on the trajectory of the ultrasound beam such as the superior temporal gyrus (fig.3b, sub-panel *iii*) and fundus of the superior temporal sulcus (fig.3b, sub-panel *ii*) or of the inferior temporal gyrus which was just ventral to the TUS trajectory (fig.3b, sub-panel *iv)*. Similarly, we measured changes in coupling between four control areas and the rest of the brain in a control state and after TUS targeted to ACC. These areas were located in between the transducer and the ACC target (fig.3c, sub-panel *iii*), on the other side of the target region (fig.3c, sub-panel *v*) as well as areas immediately rostral (fig.3c, sub-panel *ii*) and caudal (fig.3c, sub-panel *iv*) to the target region. ACC sonication had little effect on the region between the target and the transducer (fig.3ciii) and a region just anterior to the target (fig.3cii) suggesting, once again, a considerable degree of focality in the effect on neural activity. In line with the whole-brain analysis (fig.3a), and with the simulations of acoustic intensity (fig.1f), we confirmed that there were some changes in the connectional profile of a region along the stimulation trajectory just ventral to the target (fig.3c, *v*).

After confirming the focality of the direct impact of TUS (fig.3a), matching the estimated contours of the acoustic intensity (fig.1f), we considered that areas outside the directly sonicated region, but strongly connected to it, might exhibit a network-derived effect of TUS. Indeed, changes to the connectional profile of an area just posterior (fig.3c, *iv*) to the target region (fig.3c, *ii*), could be suggestive of such a network-effect. Accordingly, an additional analysis was conducted to test whether changes in areas outside the sonicated region were due to their spatial proximity to the target area or the anatomical connections they shared with the target area. When we investigated an area – the SMA – which is at a similar Euclidean distance from the target ACC region (fig.S2a) as the more caudal cingulate area 24ab, but less strongly connected to it, there were no changes (fig.S2b) in the way in which its activity was coupled with that in other brain areas. This was in contrast with changes in activity coupling of area 24ab (fig.S2c), which is more strongly connected to the ACC target compared to SMA (fig.S2b).

Effect of amygdala and ACC TUS on the auditory system

It has recently been suggested that TUS's impact on neural activity is mediated by its auditory impact (Guo et al., 2018; Sato et al., 2018). Several considerations suggest that it might not be

possible to explain away the current findings as the result of an auditory artefact. First, the auditory impact of TUS is likely a function of specific features of its frequency and pulse type, and especially of the frequency used to modulate the ultrasonic carrier wave. Second, the auditory stimulation associated with the TUS application ceased after the 40 s sonication period but the neural activity measurements were initiated tens of minutes later. Third, TUS of each area, ACC and amygdala, had specific effects that were distinct to one another. The only amygdala activity relationship affected by ACC TUS was that between amygdala and ACC and the only ACC activity relationship affected by amygdala TUS was that between ACC and amygdala.

Nevertheless, we also carried out a fourth line of inquiry and examined whether it is plausible that an auditory effect could have mediated the TUS effects on amygdala and ACC. To quantify this probability, we correlated any TUS effects on primary auditory cortex (A1) connectivity with TUS effects on the targeted regions (fig.4a). TUS effects on the auditory cortex after both amygdala ($r=0.1084$, $p=0.7007$) and ACC ($r=0.1474$, $p=0.6000$) sonication are unrelated to the TUS effects at each target site and are therefore unlikely to have mediated effects seen at the stimulation sites. However, it is possible that TUS over amygdala or ACC had an impact on A1 connectivity separately from its impact on the stimulated sites themselves (fig.4b). While A1 connectivity is not impacted by ACC TUS (fig.4b, non-parametric permutation test, $p=0.6871$), amygdala TUS did have a significant impact on A1 connectivity (fig.4b, non-parametric permutation test, $p = 0.0002$). Closer inspection revealed that this was due to a diminution solely in A1's interactions with the amygdala itself and two areas with which the amygdala is itself strongly connected with: ACC and orbitofrontal cortex. Differential effects of ACC and amygdala TUS on A1 connectivity might be driven by some direct, albeit weak, connections of amygdala with A1 (Yukie, 2002). Similarly, given amygdala's strong connections to ACC and orbitofrontal cortex, it is perhaps not surprising that amygdala sonication might affect A1's interactions with them. Importantly, these circumscribed effects on A1 connectivity are not predictive of the effects elsewhere. In summary, the alteration seen in the A1 fingerprint is a poor match to the alteration seen in the amygdala fingerprint after amygdala TUS or in the ACC fingerprint after ACC TUS.

DISCUSSION

In these investigations we combined TUS with resting-state fMRI to examine the impact of modulating activity in subcortical and deep cortical areas of the primate brain. Experiments 1 and 2 revealed dissociable effects of amygdala and ACC TUS. The dissociable nature of the effects and the fact that they were observed more than an hour after the 40 s stimulation period suggests they are not mediated by the stimulation's auditory impact (Guo et al., 2018; Sato et al., 2018). In each case

effects were apparent as reductions in activity coupling between the stimulated area and other regions with which it is normally interconnected; after TUS, a brain area's activity appears to be driven less by activity in the areas with which it is connected and more so by the artificial modulation induced by TUS.

Any impact that TUS exerts on the auditory system is likely to depend on the precise details of the sonication frequency, pulse/modulation frequency, and pulse shape and might be specific to other features of the preparation such as anesthesia level (Airan and Pauly, 2018). Here we employed an ultrasound frequency of 250kHz that we pulse modulated at 10Hz: as such we ensured that both the ultrasound carrier wave and the wave envelope frequency are well outside of the macaque hearing range. This can be contrasted against more conventional protocols where the ultrasound is pulse modulated at ~1kHz, within the audible range of both rodents and primates. Moreover, the "offline" stimulation protocol we employed also made it less likely that the auditory system was stimulated at the time that neural activity was recorded; neural activity was only measured many minutes after the cessation of a 40 s period of TUS.

Our aim in the current study was to examine whether TUS can modulate neural activity. The results obtained demonstrate that TUS can exert a relatively focal and circumscribed impact on neural activity. However, as a consequence of using a recording technique that is sensitive to a number of neurophyiological processes, it was not possible to establish the precise nature of the neurophysiological process that mediated the fMRI signal effects that we observed. It is possible that TUS may act not simply by immediately inducing or reducing activity in neurons but by modulating their responsiveness to other neural inputs; thus its effect may have been more easily detected by an analysis strategy such as the current one that focused on measuring the relationship between activity in the stimulated area and elsewhere. As with other repetitive neurostimulation protocols it is also possible that TUS's offline effects are partly driven by the induction of plastic changes, with long-term-potentiation/depression-like characteristics, and again this might have implications for how its effects are best detected.

Several molecular mechanisms describing how low-intensity ultrasound stimulation modulates neuronal activity have been suggested. However, recent investigations on the interactions between sound pressure waves and brain tissue suggest that ultrasound primarily exerts its modulatory effects through a mechanical action on cell membranes, notably affecting ion channel gating (Kubanek et al., 2016; Prieto et al., 2013; Tyler et al., 2008). While the precise mechanisms are being determined (Kubanek, 2018; Kubanek et al., 2018; Tyler et al., 2018) the current results suggest TUS may be suitable as a tool for focal manipulation of activity in many brain

areas in primates. Specifically, they show that TUS may even be used to manipulate activity in subcortical structures in monkeys.

TUS's capacity to stimulate subcortical and deep cortical areas in primates, therefore, opens the prospect of advanced non-invasive causal brain mapping. To date, non-invasive manipulation of brain activity in humans can be done reversibly only using neuromodulation methods such as transcranial magnetic stimulation and transcranial current stimulation. However, the spatial resolution of some of these techniques is limited (Walsh and Cowey, 2000; Dayan et al., 2013). Even more critically, application of these techniques is constrained to the surface of the brain as their efficacy falls off rapidly with depth.

Before it becomes possible to use repetitive TUS to study the human brain in a routine manner, a number of considerations must be borne in mind. It will be important to establish the safety of the technique. In another recent study we have shown that TUS of the type used here causes no permanent damage to tissue on histological analysis (Verhagen et al., bioRxiv). Structural MRI scans collected shortly after TUS in the present study showed no evidence of transient edema (Fig.S4). While such results are encouraging, further studies may be needed to establish if this remains true even after a greater number of TUS sessions, after TUS sessions of longer duration, or after TUS at a greater intensity. Care may need to be taken with the assessment of each new protocol that is devised. Before the technique is used routinely in human cognitive neuroscience experiments, it should be noted that its neural effects may be sustained over a period of time that is substantially longer than in many laboratory experiments (Verhagen et al., bioRxiv); care will therefore need to be taken in deciding when a human participant might leave the laboratory and travel home. In addition, sonication appears to impact on the meninges (Verhagen et al., bioRxiv) and the full nature of this impact may need to be established. Not only does this have safety implications but it also suggests that the impact of TUS to a brain area is best assessed by comparison to the impact of TUS to an appropriate control site.

In summary, based on the results reported here, TUS can be used to transiently and reversibly alter neural activity in subcortical and deep cortical areas with high spatial specificity. To date, it is the most promising neuromodulatory technique to reach areas deep below the dorsolateral surface of the brain in a minimally invasive and focal manner, thereby providing it with the potential for causally mapping brain functions within and across species. While it may currently lack the capacity to target specific neurons, as do some optogenetic and chemogenetic techniques (Khatoun et al., 2017; Sternson and Roth, 2014; Tang et al., 2018; Yizhar et al., 2011), it may provide a method for investigating brain areas that may make it suitable for use with primate species, which are rarely investigated with such techniques even though many brain areas are particularly well

developed or only present in primates (Passingham and Wise, 2012). With care it may even be possible to employ offline TUS protocols in investigations of human brain function.

Contributions

D.F. and J.S. designed the experiment; D.F. and J.S. collected the data; D.F., L.V., M.F.S.R., and J.S. analyzed the data; L.V. and R.B.M. contributed analysis tools; J.F.A., C.C, and D.F. contributed to the ultrasound modelling; D.F., L.V., E.F., M.F.S.R., J.F.A., and J.S. wrote the manuscript.

Acknowledgements

Funding for this study was provided by a Wellcome Senior Investigator Award (WT100973AIA), MRC programme grant (MR/P024955/1), MRC programme grant (G0902373), Wellcome Trust Henry Dale Fellowship (105651/Z/14/Z), Wellcome Trust UK Grant (105238/Z/14/Z), The Wellcome Centre for Integrative Neuroimaging (203139/Z/16/Z), BBRSC grant (BB/N019814/1), NWO grant (452-13-015), Bettencourt Schueller Foundation and the "Agence Nationale de la Recherche" under the program ‘‘Future Investments’’ (ANR-10-EQPX-15).

Declaration of Interests

The authors have no competing interests to declare.

References

Airan, R.D., Pauly, K.B., 2018. Hearing out Ultrasound Neuromodulation. Neuron 98, 875–877. https://doi.org/10.1016/j.neuron.2018.05.031

Caspari, N., Arsenault, J.T., Vandenberghe, R., Vanduffel, W., 2018. Functional Similarity of Medial Superior Parietal Areas for Shift-Selective Attention Signals in Humans and Monkeys. Cereb. Cortex 28, 2085–2099. https://doi.org/10.1093/cercor/bhx114

Constans, C., Deffieux, T., Pouget, P., Tanter, M., Aubry, J.-F., 2017. A 200–1380-kHz Quadrifrequency Focused Ultrasound Transducer for Neurostimulation in Rodents and Primates: Transcranial In Vitro Calibration and Numerical Study of the Influence of Skull Cavity. IEEE Trans. Ultrason. Ferroelectr. Freq. Control 64, 717–724. https://doi.org/10.1109/TUFFC.2017.2651648

Dallapiazza, R.F., Timbie, K.F., Holmberg, S., Gatesman, J., Lopes, M.B., Price, R.J., Miller, G.W., Elias, W.J., 2018. Noninvasive neuromodulation and thalamic mapping with low-intensity focused ultrasound. J. Neurosurg. 128, 875–884. https://doi.org/10.3171/2016.11.JNS16976

Dayan, E., Censor, N., Buch, E.R., Sandrini, M., Cohen, L.G., 2013. Noninvasive brain stimulation: from physiology to network dynamics and back. Nat. Neurosci. 16, 838–844. https://doi.org/10.1038/nn.3422

Deffieux, T., Younan, Y., Wattiez, N., Tanter, M., Pouget, P., Aubry, J.-F., 2013. Low-Intensity Focused Ultrasound Modulates Monkey Visuomotor Behavior. Curr. Biol. 23, 2430–2433. https://doi.org/10.1016/j.cub.2013.10.029

Duff, E.P., Makin, T., Cottaar, M., Smith, S.M., Woolrich, M.W., 2018. Disambiguating brain functional connectivity. NeuroImage 173, 540–550. https://doi.org/10.1016/j.neuroimage.2018.01.053

Fomenko, A., Neudorfer, C., Dallapiazza, R.F., Kalia, S.K., Lozano, A.M., 2018. Low-intensity ultrasound neuromodulation: An overview of mechanisms and emerging human applications. Brain Stimul. Basic Transl. Clin. Res. Neuromodulation 11, 1209–1217. https://doi.org/10.1016/j.brs.2018.08.013

Ghahremani, M., Hutchison, R.M., Menon, R.S., Everling, S., 2017a. Frontoparietal Functional Connectivity in the Common Marmoset. Cereb. Cortex 27, 3890–3905. https://doi.org/10.1093/cercor/bhw198

Ghahremani, M., Hutchison, R.M., Menon, R.S., Everling, S., 2017b. Frontoparietal Functional Connectivity in the Common Marmoset. Cereb. Cortex N. Y. N 1991 27, 3890–3905. https://doi.org/10.1093/cercor/bhw198

Glasser, M.F., Sotiropoulos, S.N., Wilson, J.A., Coalson, T.S., Fischl, B., Andersson, J.L., Xu, J., Jbabdi, S., Webster, M., Polimeni, J.R., Van Essen, D.C., Jenkinson, M., 2013. The minimal preprocessing pipelines for the Human Connectome Project. NeuroImage 80, 105–124. https://doi.org/10.1016/j.neuroimage.2013.04.127

Guo, H., Hamilton, M., Offutt, S.J., Gloeckner, C.D., Li, T., Kim, Y., Legon, W., Alford, J.K., Lim, H.H., 2018. Ultrasound Produces Extensive Brain Activation via a Cochlear Pathway. Neuron. https://doi.org/10.1016/j.neuron.2018.04.036

Hutchison, R.M., Womelsdorf, T., Gati, J.S., Leung, L.S., Menon, R.S., Everling, S., 2012. Resting-state connectivity identifies distinct functional networks in macaque cingulate cortex. Cereb. Cortex N. Y. N 1991 22, 1294–1308. https://doi.org/10.1093/cercor/bhr181

Jenkinson, M., Bannister, P., Brady, M., Smith, S., 2002. Improved optimization for the robust and accurate linear registration and motion correction of brain images. NeuroImage 17, 825–841.

Jenkinson, M., Smith, S., 2001. A global optimisation method for robust affine registration of brain images. Med. Image Anal. 5, 143–156.

Khatoun, A., Asamoah, B., Laughlin, M.M., 2017. Simultaneously Excitatory and Inhibitory Effects of Transcranial Alternating Current Stimulation Revealed Using Selective Pulse-Train Stimulation in the Rat Motor Cortex. J. Neurosci. 37, 9389–9402. https://doi.org/10.1523/JNEUROSCI.1390-17.2017

King, R.L., Brown, J.R., Newsome, W.T., Pauly, K.B., 2013. Effective parameters for ultrasound-induced in vivo neurostimulation. Ultrasound Med. Biol. 39, 312–331. https://doi.org/10.1016/j.ultrasmedbio.2012.09.009

Kubanek, J., 2018. Neuromodulation with transcranial focused ultrasound. Neurosurg. Focus 44, E14. https://doi.org/10.3171/2017.11.FOCUS17621

Kubanek, J., Shi, J., Marsh, J., Chen, D., Deng, C., Cui, J., 2016. Ultrasound modulates ion channel currents. Sci. Rep. 6, 24170. https://doi.org/10.1038/srep24170

Kubanek, J., Shukla, P., Das, A., Baccus, S.A., Goodman, M.B., 2018. Ultrasound Elicits Behavioral Responses through Mechanical Effects on Neurons and Ion Channels in a Simple Nervous System. J. Neurosci. 38, 3081–3091. https://doi.org/10.1523/JNEUROSCI.1458-17.2018

Margulies, D.S., Ghosh, S.S., Goulas, A., Falkiewicz, M., Huntenburg, J.M., Langs, G., Bezgin, G., Eickhoff, S.B., Castellanos, F.X., Petrides, M., Jefferies, E., Smallwood, J., 2016. Situating the

default-mode network along a principal gradient of macroscale cortical organization. Proc. Natl. Acad. Sci. 113, 12574–12579. https://doi.org/10.1073/pnas.1608282113

Margulies, D.S., Vincent, J.L., Kelly, C., Lohmann, G., Uddin, L.Q., Biswal, B.B., Villringer, A., Castellanos, F.X., Milham, M.P., Petrides, M., 2009. Precuneus shares intrinsic functional architecture in humans and monkeys. Proc. Natl. Acad. Sci. 106, 20069–20074. https://doi.org/10.1073/pnas.0905314106

Mars, R. B., Sallet, J., Neubert, F.-X., Rushworth, M.F.S., 2013. Connectivity profiles reveal the relationship between brain areas for social cognition in human and monkey temporoparietal cortex. Proc. Natl. Acad. Sci. 110, 10806–10811. https://doi.org/10.1073/pnas.1302956110

Mars, R.B., Verhagen, L., Gladwin, T.E., Neubert, F.-X., Sallet, J., Rushworth, M.F.S., 2016. Comparing brains by matching connectivity profiles. Neurosci. Biobehav. Rev. 60, 90–97. https://doi.org/10.1016/j.neubiorev.2015.10.008

Munuera, J., Rigotti, M., Salzman, C.D., 2018. Shared neural coding for social hierarchy and reward value in primate amygdala. Nat. Neurosci. 21, 415–423. https://doi.org/10.1038/s41593-018-0082-8

Neubert, F.-X., Mars, R.B., Sallet, J., Rushworth, M.F.S., 2015. Connectivity reveals relationship of brain areas for reward-guided learning and decision making in human and monkey frontal cortex. Proc. Natl. Acad. Sci. 112, E2695–E2704. https://doi.org/10.1073/pnas.1410767112

Neubert, F.-X., Mars, R.B., Thomas, A.G., Sallet, J., Rushworth, M.F.S., 2014. Comparison of Human Ventral Frontal Cortex Areas for Cognitive Control and Language with Areas in Monkey Frontal Cortex. Neuron 81, 700–713. https://doi.org/10.1016/j.neuron.2013.11.012

Noonan, M.P., Sallet, J., Mars, R.B., Neubert, F.X., O'Reilly, J.X., Andersson, J.L., Mitchell, A.S., Bell, A.H., Miller, K.L., Rushworth, M.F.S., 2014. A Neural Circuit Covarying with Social Hierarchy in Macaques. PLoS Biol. 12, e1001940. https://doi.org/10.1371/journal.pbio.1001940

O'Reilly, J.X., Croxson, P.L., Jbabdi, S., Sallet, J., Noonan, M.P., Mars, R.B., Browning, P.G.F., Wilson, C.R.E., Mitchell, A.S., Miller, K.L., Rushworth, M.F.S., Baxter, M.G., 2013. Causal effect of

disconnection lesions on interhemispheric functional connectivity in rhesus monkeys. Proc. Natl. Acad. Sci. U. S. A. 110, 13982–13987. https://doi.org/10.1073/pnas.1305062110

Passingham, R.E., Stephan, K.E., Kötter, R., 2002. The anatomical basis of functional localization in the cortex. Nat. Rev. Neurosci. 3, 606–616. https://doi.org/10.1038/nrn893

Passingham, R.E., Wise, S.P., 2012. The neurobiology of the prefrontal cortex: anatomy, evolution, and the origin of insight, 1st ed. ed, Oxford psychology series. Oxford University Press, Oxford, United Kingdom.

Prieto, M.L., Ömer, O., Khuri-Yakub, B.T., Maduke, M.C., 2013. Dynamic response of model lipid membranes to ultrasonic radiation force. PloS One 8, e77115. https://doi.org/10.1371/journal.pone.0077115

Procyk, E., Wilson, C.R.E., Stoll, F.M., Faraut, M.C.M., Petrides, M., Amiez, C., 2016. Midcingulate Motor Map and Feedback Detection: Converging Data from Humans and Monkeys. Cereb. Cortex N. Y. NY 26, 467–476. https://doi.org/10.1093/cercor/bhu213

Reveley, C., Gruslys, A., Ye, F.Q., Glen, D., Samaha, J., E Russ, B., Saad, Z., K Seth, A., Leopold, D.A., Saleem, K.S., 2017. Three-Dimensional Digital Template Atlas of the Macaque Brain. Cereb. Cortex N. Y. N 1991 27, 4463–4477. https://doi.org/10.1093/cercor/bhw248

Sallet, J., Mars, R.B., Noonan, M.P., Neubert, F.-X., Jbabdi, S., O'Reilly, J.X., Filippini, N., Thomas, A.G., Rushworth, M.F., 2013. The Organization of Dorsal Frontal Cortex in Humans and Macaques. J. Neurosci. 33, 12255–12274. https://doi.org/10.1523/JNEUROSCI.5108-12.2013

Sato, T., Shapiro, M.G., Tsao, D.Y., 2018. Ultrasonic Neuromodulation Causes Widespread Cortical Activation via an Indirect Auditory Mechanism. Neuron. https://doi.org/10.1016/j.neuron.2018.05.009

Shen, H.H., 2015. Core Concept: Resting-state connectivity. Proc. Natl. Acad. Sci. 112, 14115–14116. https://doi.org/10.1073/pnas.1518785112

Shen, K., Hutchison, R.M., Bezgin, G., Everling, S., McIntosh, A.R., 2015. Network Structure Shapes Spontaneous Functional Connectivity Dynamics. J. Neurosci. 35, 5579–5588. https://doi.org/10.1523/JNEUROSCI.4903-14.2015

Smith, S.M., 2002. Fast robust automated brain extraction. Hum. Brain Mapp. 17, 143–155. https://doi.org/10.1002/hbm.10062

Smith, S.M., Hyvärinen, A., Varoquaux, G., Miller, K.L., Beckmann, C.F., 2014. Group-PCA for very large fMRI datasets. NeuroImage 101, 738–749. https://doi.org/10.1016/j.neuroimage.2014.07.051

Sternson, S.M., Roth, B.L., 2014. Chemogenetic Tools to Interrogate Brain Functions. Annu. Rev. Neurosci. 37, 387–407. https://doi.org/10.1146/annurev-neuro-071013-014048

Tang, A.D., Bennett, W., Hadrill, C., Collins, J., Fulopova, B., Wills, K., Bindoff, A., Puri, R., Garry, M.I., Hinder, M.R., Summers, J.J., Rodger, J., Canty, A.J., 2018. Low intensity repetitive transcranial magnetic stimulation modulates skilled motor learning in adult mice. Sci. Rep. 8, 4016. https://doi.org/10.1038/s41598-018-22385-8

Tufail, Y., Yoshihiro, A., Pati, S., Li, M.M., Tyler, W.J., 2011. Ultrasonic neuromodulation by brain stimulation with transcranial ultrasound. Nat. Protoc. 6, 1453–1470. https://doi.org/10.1038/nprot.2011.371

Tyler, W.J., Lani, S.W., Hwang, G.M., 2018. Ultrasonic modulation of neural circuit activity. Curr. Opin. Neurobiol. 50, 222–231. https://doi.org/10.1016/j.conb.2018.04.011

Tyler, W.J., Tufail, Y., Finsterwald, M., Tauchmann, M.L., Olson, E.J., Majestic, C., 2008. Remote Excitation of Neuronal Circuits Using Low-Intensity, Low-Frequency Ultrasound. PLoS ONE 3, e3511. https://doi.org/10.1371/journal.pone.0003511

Van Essen, D.C., 2002. Surface-based atlases of cerebellar cortex in the human, macaque, and mouse. Ann. N. Y. Acad. Sci. 978, 468–479.

Van Essen, D.C., Dierker, D.L., 2007. Surface-Based and Probabilistic Atlases of Primate Cerebral Cortex. Neuron 56, 209–225. https://doi.org/10.1016/j.neuron.2007.10.015

Van Hoesen, G.W., Morecraft, R.J., Vogt, B.A., 1993. Connections of the Monkey Cingulate Cortex, in: Neurobiology of Cingulate Cortex and Limbic Thalamus. Birkhäuser, Boston, MA, pp. 249–284. https://doi.org/10.1007/978-1-4899-6704-6_9

Vincent, J.L., Patel, G.H., Fox, M.D., Snyder, A.Z., Baker, J.T., Van Essen, D.C., Zempel, J.M., Snyder, L.H., Corbetta, M., Raichle, M.E., 2007. Intrinsic functional architecture in the anaesthetized monkey brain. Nature 447, 83–86. https://doi.org/10.1038/nature05758

Walsh, V., Cowey, A., 2000. Transcranial magnetic stimulation and cognitive neuroscience. Nat. Rev. Neurosci. 1, 73–80. https://doi.org/10.1038/35036239

Yizhar, O., Fenno, L.E., Davidson, T.J., Mogri, M., Deisseroth, K., 2011. Optogenetics in Neural Systems. Neuron 71, 9–34. https://doi.org/10.1016/j.neuron.2011.06.004

Yoo, S.-S., Bystritsky, A., Lee, J.-H., Zhang, Y., Fischer, K., Min, B.-K., McDannold, N.J., Pascual-Leone, A., Jolesz, F.A., 2011. Focused ultrasound modulates region-specific brain activity. NeuroImage 56, 1267–1275. https://doi.org/10.1016/j.neuroimage.2011.02.058

Yukie, M., 2002. Connections between the amygdala and auditory cortical areas in the macaque monkey. Neurosci. Res. 42, 219–229.

Zhang, Y., Brady, M., Smith, S., 2001. Segmentation of brain MR images through a hidden Markov random field model and the expectation-maximization algorithm. IEEE Trans. Med. Imaging 20, 45–57. https://doi.org/10.1109/42.906424

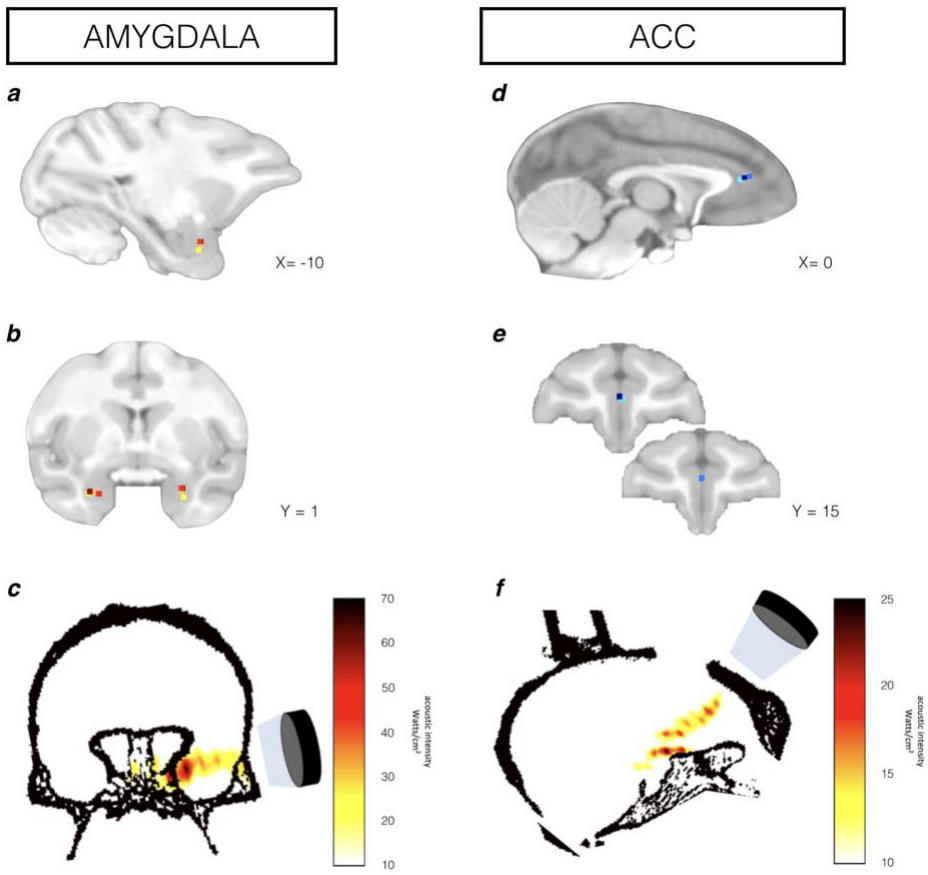

1. Stimulation targets. Stimulation target position is shown for each individual animal (colored dots) on sagittal and coronal views for TUS targeted at amygdala (**a-b**) and ACC (**d-e**). Acoustic intensity field (Watts/cm^2) generated by the ultrasound beam in the brain is shown for one example animal per TUS target, amygdala (coronal plane **c;** maximum spatial peak pulse average intensity (I_{sppa}) in focal region= 64.9 W/cm^2; spatial peak temporal average intensity ($I_{spta)}$= 19.5 W/cm^2; max pressure=1.44 MPa) and ACC (sagittal plane f; maximum I_{sppa} in focal region=18.8 W/cm^2; I_{spta} = 5.63 W/cm^2; max pressure=0.78 MPa). The target position can be delineated with accuracy in all animals in panels a, b, d, and e by using each individual's own MRI scan. As a result, the activity and functional connectivity of the target areas can be examined accurately in each animal (see subsequent figures and supplementary materials). However, some slight imprecision in the estimation in the acoustic intensity maps in panels c and f may occur; this is because group average targets are used in conjunction with the computed tomography X-ray scan of a single individual during the modelling.

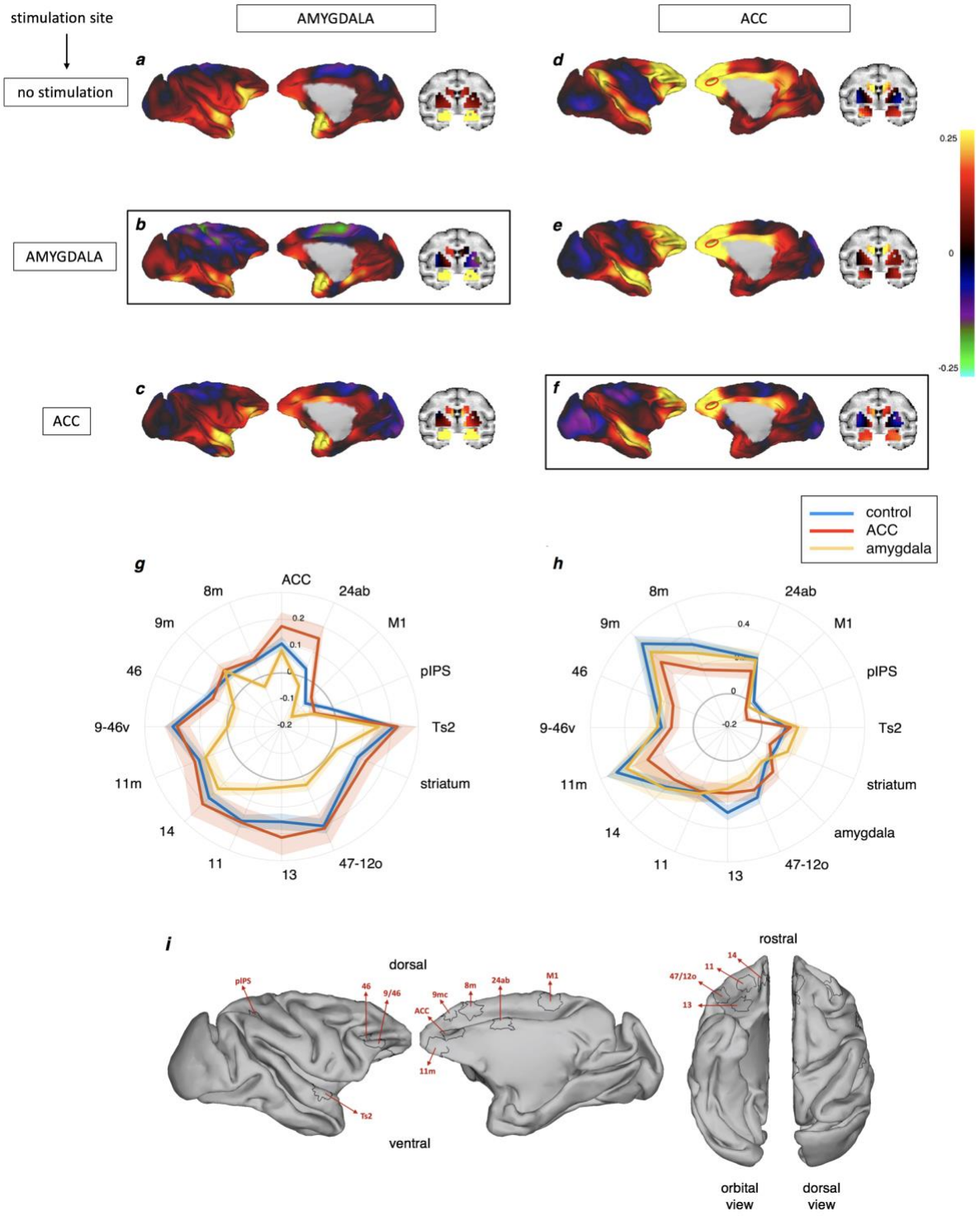

2. Amygdala and ACC functional coupling changes after stimulation. Panels a, b, and c on the left side of the figure show activity coupling between amygdala (seed masked in yellow) and the rest of the brain in no stimulation/control condition (**a**), after amygdala TUS (**b**), and after ACC TUS (**c**). Panels d, e, f show activity coupling between ACC (circled in red) and the rest of the brain in no stimulation/control condition (**d**), after amygdala TUS (**e**), and after ACC TUS (**f**). Hot colors indicate

positive coupling (Fisher's z). Functional connectivity from TUS-targeted regions are highlighted by black boxes. Each type of TUS had a selective effect on the stimulated area: amygdala coupling was strongly changed by amygdala TUS only (b) and ACC coupling was strongly changed by ACC TUS only (f). Areas showing changes in coupling with TUS-targeted regions after TUS are circled in black and compared with the other 2 control conditions. The 4mm spherical ROIs used in the statistical tests are highlighted in figure **i** on a lateral, medial, orbital and dorsal view. The lines in the left panel indicates the strength of activity coupling between amygdala (**g**) and other brain areas labelled on the circumference in control animals (blue), after amygdala TUS (yellow), and after ACC TUS (red). The lines in the right panel show activity coupling between ACC (**h**) and the rest of the brain in control animals (blue), after ACC TUS (red), and after amygdala TUS (yellow). Each type of TUS had a selective effect on the stimulated area: amygdala coupling was strongly affected by amygdala TUS (the yellow line is closer to the center of the panel than the blue line) and ACC coupling was strongly disrupted by ACC TUS (the red line is closer to the center of the panel than the blue line). Standard error of the mean is indicated by shading around each line.

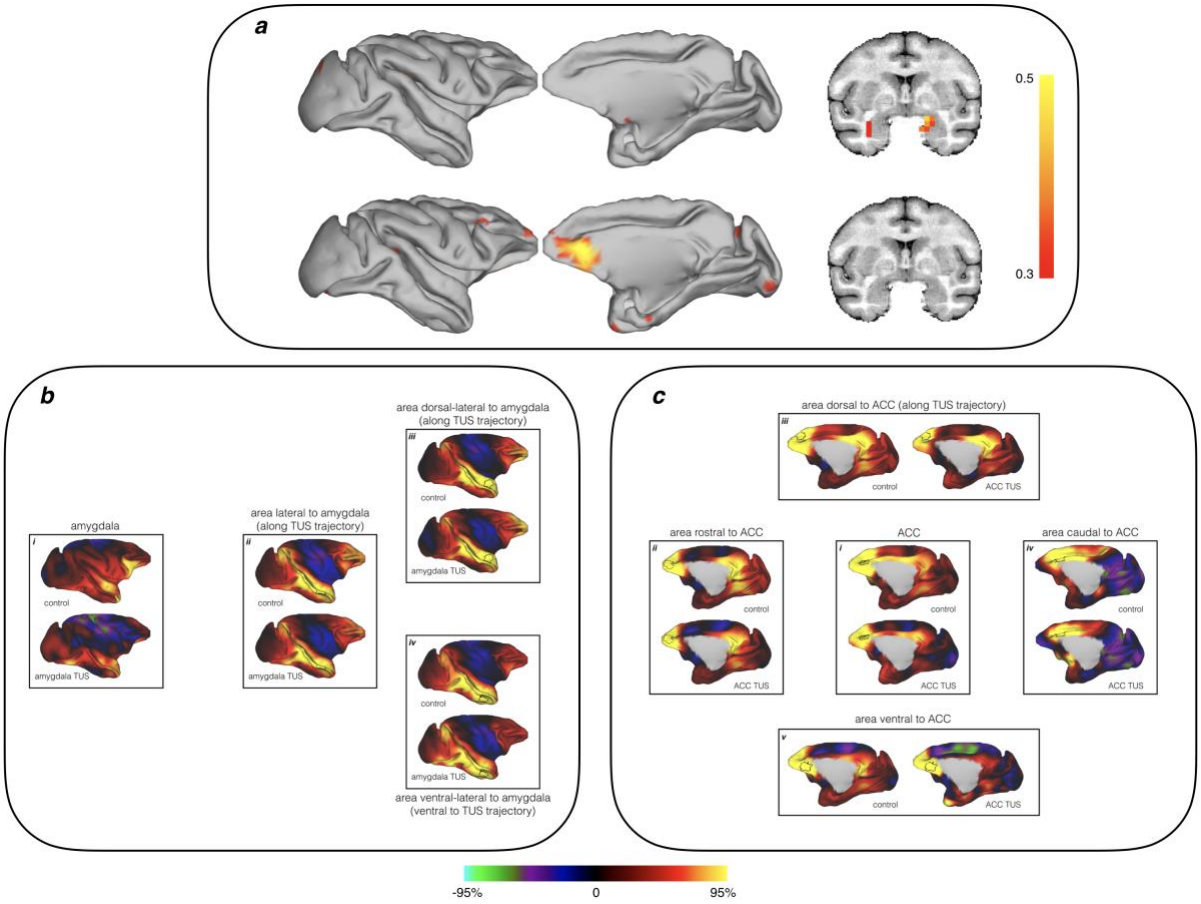

3. Spatial extent of the TUS neuromodulatory effect and its impact on areas neighboring the stimulated region. *Panel a*; amplitude and spatial extent of the impact of amygdala TUS (top row) and ACC TUS (bottom row) on the coupling of each point in the brain with the same set of a priori defined areas used in figure 2g,h. Hot colors indicate a strong decrement in coupling after TUS compared to the control state (delta Fisher's z). The effect of TUS on activity coupling was restricted to the amygdala after amygdala TUS and to the ACC and regions immediately ventral along the ultrasound trajectory following ACC TUS (bottom row). *Panel b;* as also shown in figure 2, the whole brain coupling of the amygdala target region (sub-panel *i*; the outline in black in all cases indicates the regions for which the whole-brain connectivity is shown) is significantly different in the control condition and when TUS is applied to amygdala. Hot colors indicate positive coupling (Fisher's z). Sub-panels *ii*, *iii*, *iv* show the activity coupling of regions along (*ii*,*iii*) or immediately surrounding the trajectory of the ultrasound stimulation beam (*iv*), in the control condition and after amygdala TUS. There were no changes in the coupling of these regions and the rest of the brain. This is true for the regions through which the stimulation trajectory passed in the fundus of the superior temporal sulcus (*ii*) and the superior temporal gyrus (*iii*) or in the immediately adjacent inferior temporal gyrus (*iv*). *Panel c*; the whole brain coupling of the ACC target region (*i*) is significantly different in the control condition and when TUS is applied to ACC. Sub-panels *ii*, *iii*, *iv* and *v* show the activity

coupling of regions near the ACC target in both the ACC TUS and control conditions. This includes areas located along the trajectory of the ultrasound stimulation beam such as (*iii*) the area in between the transducer and the target region in ACC and the area on the other side of the target region (*v*) as well as areas immediately rostral (*ii*) and caudal (*iv*) to the target region. Some changes in coupling can be seen along the stimulation trajectory in the area just ventral to the target (*v*) and also in an area which is unlikely to have been hit directly by the ultrasound beam (*iv*). These areas are strongly anatomically connected with the targeted area.

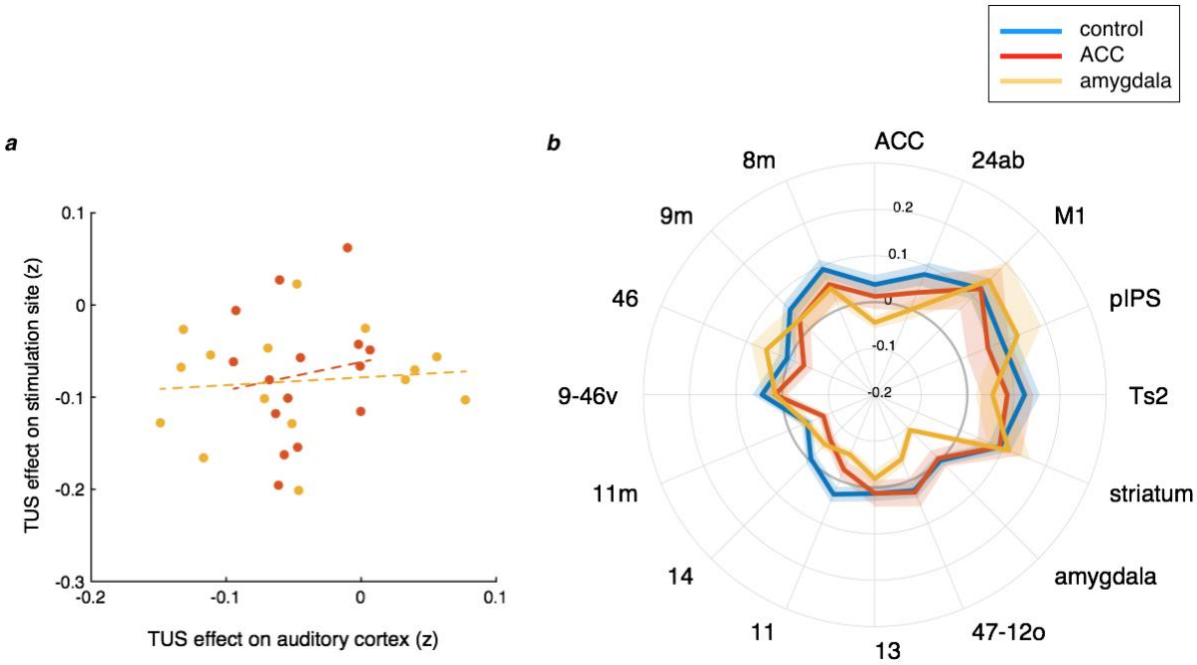

4. Effect of amygdala and ACC TUS on the functional coupling of primary auditory cortex. *Panel a*; ACC TUS (red line) had no effects on the functional coupling of A1. Amygdala TUS (yellow line) affected the relationship between A1's activity and activity in several areas that are linked to the A1 via the amygdala including the amygdala itself, lateral orbitofrontal cortex area 47/12o and ACC. *Panel b*; TUS effects on the auditory cortex after neither amygdala (yellow) nor ACC (red) cannot explain the TUS effect on the respective stimulation sites.

STAR *METHODS

KEY RESOURCE TABLE

REAGENT or RESOURCE	SOURCE	IDENTIFIER
Chemicals, Peptides, and Recombinant Proteins		
Isoflurane – ISOFLO 250ml	Centaur	30135687
Ketamine – Narketan 10% 10ml INJ CD(SCH4)1 1-MCD	Centaur	03120257
Midazolam – Hypnoval amps 10mg/2ml	Centaur	23191407
Atropine – Atrocare INJ 25ml	Centaur	01300236
Meloxicam – Metacam INJ 10ml 5mg/ml DOGS/CATS	Centaur	02500456
Ranitidine 50mg/2ml x5 INJ	Centaur	30294115
Saline	DPAG, University of Oxford	N/A
Formalin	DPAG, University of Oxford	N/A
SignaGel Electrode Gel	Parker Laboratories	#15-25
Experimental Models: Organisms/Strains		
Macaca mulatta, 9 males, 2 females, between 4-11 years old, between 7-15 kg, socially housed	MRC, Centre for Macaques	NCBITaxon:9544
Software and Algorithms		
MATLAB 2017a	Mathworks	RRID: SCR_001622
FMRIB Software Library v5.0	FMRIB, WIN, Oxford, UK	RRID:SCR_002823
Connectome Workbench	The Human Connectome Project and Connectome Coordination Facility	RRID:SCR_008750
Magnetic Resonance Comparative Anatomy Toolbox	Neuroecology Lab	https://github.com/neuroecology/MrCat
Other		
Transducer H-115MR 250kHz SN:018	Sonic Concepts	www.sonicconcepts.com
Transducer H-115MR 250kHz SN:017	Sonic Concepts	www.sonicconcepts.com
Amplifier Model 75A250A – 75Watts – 10khz 250MHz	Amplifier Research	www.arworld.us
Tie Pie Handyscope HS5 SN: 32239	Tie Pie	https://www.tiepie.com
Brainsight frameless stereotaxic neuronavigation system	Rogue Research	RRID:SCR_009539
MRI compatible frame	Crist Instruments	http://www.cristinstrument.com/products/stereotax/stereotax-primate
four-channel phased-array coil	Windmiller Kolster Scientific	https://www.wkscientific.com/#mri-coils

METHODS DETAILS

Ultrasound stimulation

A single-element ultrasound transducer (H115-MR, diameter 64 mm, Sonic Concept, Bothell, WA, USA) with a 51.74 mm focal depth was used with region-specific coupling cones filled with degassed water and sealed with a latex membrane (Durex) to assess TUS of ACC (experiment 1; n=3) and amygdala (experiment 2; n=4) (fig.1). The ultrasound wave frequency was set to the 250 kHz resonance frequency and 30 ms bursts of ultrasound were generated every 100 ms (duty cycle 30%) with a digital function generator (Handyscope HS5, TiePie engineering, Sneek, the Netherlands). Overall, the stimulation lasted for 40 s. A 75-Watt amplifier (75A250A, Amplifier Research, Souderton, PA) was used to deliver the required power to the transducer. A TiePie probe (Handyscope HS5, TiePie engineering, Sneek, The Netherlands) connected to an oscilloscope was used to monitor the voltage delivered. The recorded peak-to-peak voltage was constantly maintained throughout the stimulation. Voltage values per session ranged from 128 to 134V. It corresponded to a peak negative pressure ranging from 1.15 to 1.27MPa respectively as measured in water with an in house heterodyne interferometer (Constans et al., 2017). The acoustic wave propagation of our focused ultrasound protocol was simulated at 130 V peak-to-peak voltage using finite element models of an entire monkey head to obtain estimates for the pressure amplitude, peak intensity, and spatial distribution (Constans et al., 2017). 3D maps of the skull were extracted from a monkey CT scan (0.36 mm isotropic resolution). Based on these numerical simulations, the maximum spatial peak pulse average intensity (I_{sppa}) in focal region was estimated to be 64.9 W/cm² (spatial peak temporal average intensity (I_{spta}) = 19.5 W/cm²) in the amygdala and 18.8 W/cm² (I_{spta} = 5.63 W/cm²) in ACC with a maximum pressure of 1.44 MPa in amygdala and 0.78 MPa in ACC. One train was applied to each of the more laterally situated amygdalae but a single train was applied to the midline structure (ACC) in experiments 1 and 2 respectively.

Each individual animal's structural magnetic resonance (MRI) image was registered to its head with a frameless stereotaxic neuronavigation system (Rogue Research, Montreal, CA). By recording the positions of both the ultrasound transducer and the head with an infrared tracker it was then possible to co-register the ultrasound transducer with respect to the MRI scan of the brain to position the transducer over the targeted brain region, either ACC (Procyk et al., 2016) (MNI coordinates x = 0, y = 15, z = 6) or amygdala (MNI coordinates x = -10, y = 1, z = -11; x = 9, y = 1, z = -11). The ultrasound transducer / coupling cone montage was placed directly onto previously shaved skin on which conductive gel (SignaGel Electrode; Parker Laboratories Inc.) had been applied to ensure ultrasonic coupling between the transducer and the animal's head. In the non-stimulation

condition (control), all procedures (anaesthesia, pre-scan preparation, fMRI scan acquisition and timing), with the exception of actual TUS, mirrored the TUS sessions.

Macaque rs-fMRI Data Acquisition.

Resting state fMRI (rs-fMRI) and anatomical MRI scans were collected for 11 healthy macaques (*Macaca mulatta*) (two females; rs-fMRI from nine animals were acquired under no stimulation; rs-fMRI from three animals were acquired post ACC TUS; rs-fMRI from four animals were acquired post amygdala TUS; age: 7.3 years, weight: 10.3 kg) under inhalational isoflurane anesthesia using a protocol which was previously proven successful (Noonan et al., 2014; Neubert et al., 2015) in preserving whole-brain functional connectivity as measured with BOLD signal. In the case of the TUS conditions, fMRI data collection began only after completion of the TUS train (delay between ultrasound stimulation offset and scanning onset: 37.5 minutes; SEM: 2.21 minutes). Anesthesia was induced using intramuscular injection of ketamine (10 mg/kg), xylazine (0.125– 0.25 mg/kg), and midazolam (0.1 mg/kg). Macaques also received injections of atropine (0.05 mg/kg, intramuscularly), meloxicam (0.2 mg/kg, intravenously), and ranitidine (0.05 mg/kg, intravenously). To block peripheral nerve stimulation, 15 minutes before placing the macaque in the stereotaxic frame local anaesthetic (5% lidocaine/prilocaine cream and 2.5% bupivacaine) was also administered via subcutaneous injection around the ears. The anesthetized animals were placed in an MRI-compatible stereotactic frame (Crist Instruments) in a sphinx position and placed in a horizontal 3T MRI scanner with a full-size bore. Scanning commenced 1.53 hours (SEM: 4 minutes) and 2.38 hours (SEM: 4 minutes) after anesthesia induction in TUS and control sessions, respectively. In both cases data collection commenced when the clinical peak of ketamine had passed. Anesthesia was maintained, in accordance with veterinary recommendation, using the lowest possible concentration of isoflurane to ensure that macaques were anesthetized. The depth of anesthesia was assessed and monitored using physiological parameters (heart rate and blood pressure, as well as clinical checks before the scan for muscle relaxation). During the acquisition of the functional data, the inspired isoflurane concentration was in the range 0.8–1.1%, and the expired isoflurane concentration was in the range 0.7-1%. Isoflurane was selected for the scans as it was previously demonstrated to preserve rs-fMRI networks (Neubert et al., 2015; Mars et al., 2013; Vincent et al., 2007). Macaques were maintained with intermittent positive pressure ventilation to ensure a constant respiration rate during the functional scan, and respiration rate, inspired and expired CO2, and inspired and expired isoflurane concentration were monitored and recorded using VitalMonitor software (Vetronic Services Ltd.). Core temperature and SpO2 were also constantly monitored throughout the scan.

A four-channel phased-array coil was used for data acquisition (Dr. H. Kolster, Windmiller Kolster Scientific, Fresno, CA, USA). Whole-brain BOLD fMRI data were collected from each animal for up to 78 minutes. All fMRI data were collected using the following parameters: 36 axial slices; in-plane resolution, 2 x 2 mm; slice thickness, 2 mm; no slice gap; TR, 2000 ms; TE, 19 ms; 800 volumes per run. A minimum period of 10 days elapsed between sessions.

A structural scan (average over up to three T1-weighted structural MRI images) was acquired for each macaque in the same session as the functional scans, using a T1-weighted magnetization-prepared rapid- acquisition gradient echo sequence (0.5 x 0.5 x 0.5 mm voxel resolution).

All recording and stimulation procedures were conducted under licenses from the United Kingdom (UK) Home Office in accordance with The Animals (Scientific Procedures) Act 1986 and with the European Union guidelines (EU Directive 2010/63/EU).

Macaque rs-fmri data preprocessing, and analysis.

The preprocessing and analysis of the MRI data was designed to follow the HCP Minimal Processing Pipeline (Glasser et al., 2013), using tools of FSL (https://fsl.fmrib.ox.ac.uk/fsl/fslwiki), HCP Workbench (https://www.humanconnectome.org/software/connectome-workbench), and the Magnetic Resonance Comparative Anatomy Toolbox (MrCat; www.neuroecologylab.org). The processing pipeline has been validated and described in full (Verhagen et al., BioRxiv).

The T1w images were processed in an iterative fashion cycling through brain-extraction (BET) (Smith, 2002), RF bias-field correction, and linear and non-linear registration (FLIRT and FNIRT) (Jenkinson and Smith, 2001; Jenkinson et al., 2002) to the macaca mulatta F99 atlas(Van Essen, 2002; Van Essen and Dierker, 2007). The application of robust and macaque-optimised versions of BET and FAST (Zhang et al., 2001) also provided segmentation into grey matter, white matter, and cerebral spinal fluid compartments. Segmentation of subcortical structures was obtained by registration to the D99 atlas (Reveley et al., 2017).

The first 5 volumes of the functional EPI datasets were discarded to ensure a steady RF excitation state. EPI timeseries were motion corrected using MCFLIRT. Given that the animals were anesthetized and their heads were held in a steady position, any apparent image motion, if present at all, is caused by changes to the B0 field, rather than by head motion. Accordingly, the parameter estimates from MCFLIRT can be considered to be 'B0-confound parameters' instead. Each timeseries was checked rigorously for spikes and other artefacts, both visually and using automated algorithms; where applicable slices with spikes were linearly interpolated based on temporally neighboring slices. Brain extraction, bias-correction, and registration was achieved for the functional EPI datasets

in an iterative manner, similar to the preprocessing of the structural images with the only difference that the mean of each functional dataset was registered to its corresponding T1w image using rigid-body boundary-based registration (FLIRT). EPI signal noise was reduced both in the frequency and temporal domain. First, the functional time series were high-pass filtered at 2000s. Temporally cyclical noise, for example originating from the respiratory apparatus, was removed using band-stop filters set dynamically to noise peaks in the frequency domain. Remaining temporal noise was described by the mean time course and first two subsequent principal components of the white matter (WM) and cerebral spinal fluid (CSF) compartment (considering only voxels with a high posterior probability of belonging to the WM or CSF, obtained in the T1w image using FAST). The B0-confound parameter estimates were expanded as a second degree Volterra series to capture both linear and non-linear B0 effects. Together the WM and CSF expanded B0 confound parameters were regressed out of the BOLD signal for each voxel.

The cleaned time course was then low-pass filtered with a cut-off at 10 seconds. The cleaned and filtered signal was projected from the conventional volumetric representation (2mm voxels) to the F99 cortical surface (~1.4mm spaced vertices) using Workbench command "myelin-style" mapping, while maintaining the subcortical volumetric structures. The data was spatially smoothed using a 3mm FWHM gaussian kernel, while taking into account the folding of the cortex and the anatomical boundaries of the subcortical structures. Lastly, the data were demeaned to prepare for functional connectivity analyses.

To represent subject effects, the timeseries from the three runs were concatenated to create a single timeseries per animal per intervention (control, ACC TUS, amygdala TUS). To represent group effects the run-concatenated timeseries of all animals were combined using a group-PCA approach (Smith et al., 2014) that was set to reduce the dimensionality of the data.

To construct a region-of-interest (ROI) for ACC, a circle of 4mm radius was drawn on the cortical surface around the point closest to the average stimulation coordinate (fig.1), in both the left and the right hemisphere. The same procedure was used to define other bilateral cortical regions of interest, based on literature coordinates (Neubert et al., 2015; Sallet et al., 2013; Neubert et al., 2014), to serve as targets for the fingerprint and spatial extent analyses (fig.2i). The amygdala ROI was constructed for each animal individually through non-linear registration of their T1w image to the D99 template and by subsequently resampling the (subcortical) D99 macaque atlas in native space (Reveley et al., 2017).

Coupling between the activity of each region of interest and the rest of the brain was estimated by calculating the Fisher's z-transformed correlation coefficient between each point in the ROI and all other datapoints. The resulting "connectivity-maps" were averaged across all points in

the ROI, across both hemispheres. Accordingly, the final maps represent the average coupling of a bilateral ROI with the rest of the brain. The fingerprints are obtained by extracting the average coupling with each target ROI and averaging across the two hemispheres. Statistical inference on the fingerprints was performed by using non-parametric permutation tests on cosine similarity metrics describing how similar or dissimilar pairs of fingerprints are (Mars et al., 2016)Verhagen et al., BioRxiv). The cosine similarity metric takes into account the shape of the fingerprint as a whole (but not its mean amplitude) and performs one test per pair of fingerprints, negating the necessity for correcting for multiple comparisons across fingerprint targets. In contrast to conventional parametric tests, this approach does not rely on assumptions about the shape of the distribution but will acknowledge dependencies between target ROIs in the fingerprint; as such this approach will avoid inflation of type I error. For each test we ran 10,000 permutations across individual fMRI runs to accurately approximate with high accuracy the true probability of rejecting the null-hypothesis of permutable conditions in this sample.

To examine the spatial extent of the neuromodulatory impact of TUS on activity coupling we extracted for every point in the brain, both subcortically and on the cortical surface, its average coupling strength with the fingerprint targets (fig.2i), excluding the amygdala and ACC. This approach allowed the creation of a quantified spatial map of the difference in average coupling between the control state and amygdala TUS, and between the control state and ACC TUS. For regions affected by TUS this difference will be large, while for all other regions this difference is close to zero.

Statistical inferences on the anaesthesia levels and associated physiological parameters were drawn in the context of generalized linear mixed-effects (GLME) models. These models considered the intercept, the TUS condition (control, amygdala, ACC), and the resting-state fMRI run index (1, 2, or 3) as fixed effects and the intercept and slope grouped per animal as random effects with possible correlation between them (as implemented in MATLAB, Mathworks, Natick, USA). The models were assumed to adhere to a normal distribution of the data and were fitted using Maximum-Pseudo-Likelihood estimation methods where the covariance of the random effects was approximated using Cholesky parameterization. Statistical significance was set at $\alpha = 0.05$, two-tailed, and estimated using conventional analyses of variance (ANOVA).

Supplementary Information

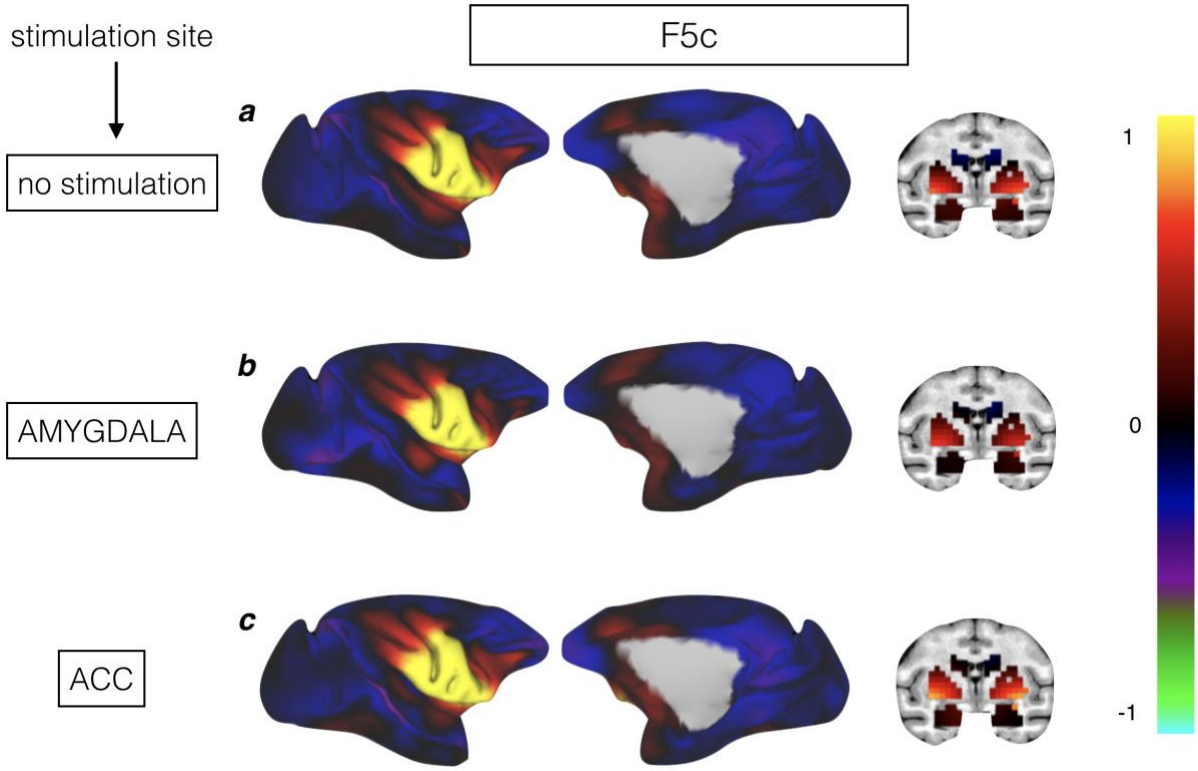

Supplementary figure 1. Whole-brain functional connectivity between stimulated and not stimulated areas with the rest of the brain. Panels a, b, and c show activity coupling between a control area, the caudal ventral premotor area F5c, and the rest of the brain in no stimulation/control condition (**a**), after amygdala TUS (**b**), and after ACC TUS (**c**). Hot colors indicate positive coupling (Fisher's z). Compared to a no stimulation condition (a), neither amygdala TUS nor ACC TUS (b,c) affected the whole-brain coupling activity of F5c which has weak anatomical connections with ACC and amygdala.

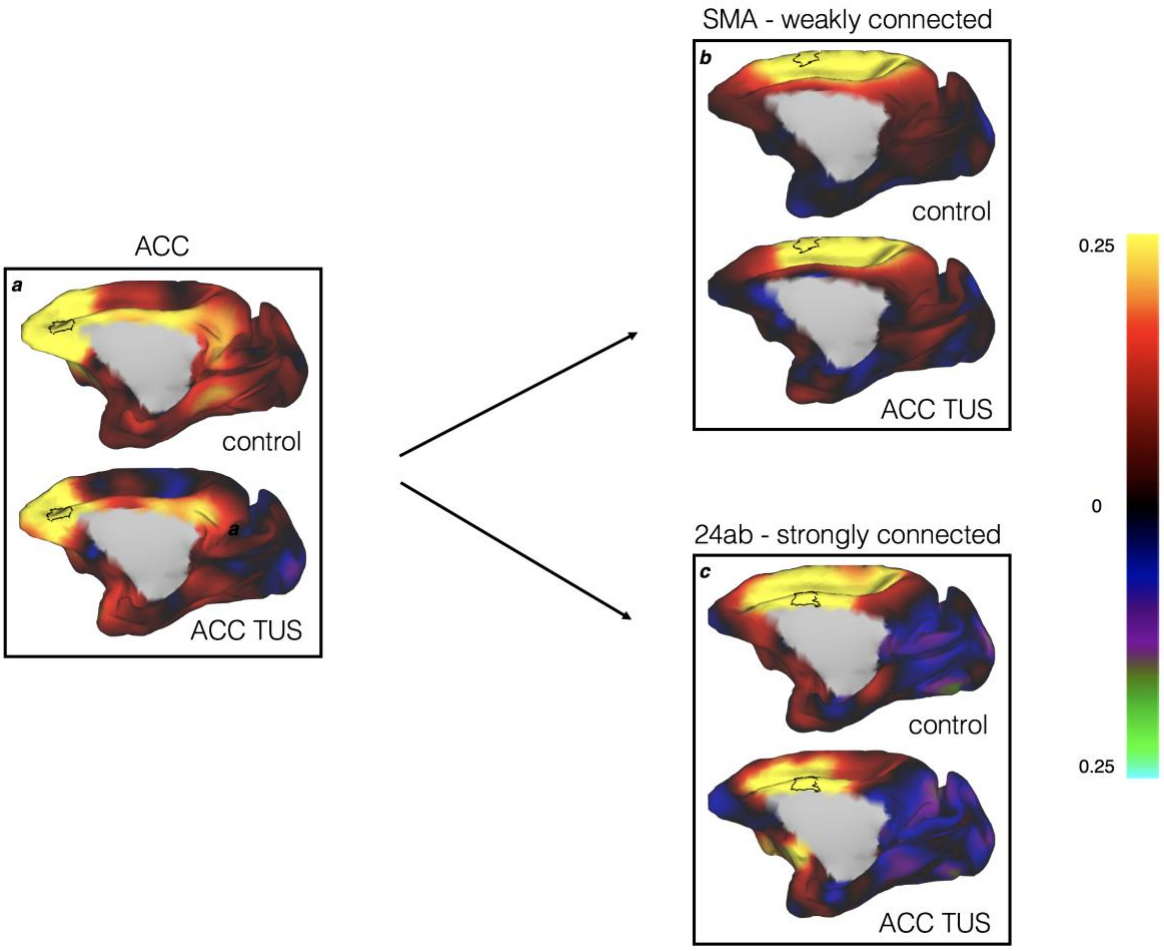

Supplementary figure 2. **Effects of TUS on regions outside the target area are mediated by the strength of anatomical connectivity rather than a result of spatial proximity.** Panels a, b, and c of the figure show whole-brain activity coupling in control and ACC TUS conditions for ACC (**a**) and two areas at an equal Euclidian distance from the ACC target region: SMA (**b**) and area 24ab (**c**). Hot colors indicate positive coupling (Fisher's z). The activity coupling of SMA, an area weakly connected with the target area ACC, and the rest of the brain is predominantly preserved after TUS. However, the whole-brain coupling of an area more strongly connected with the target ACC region (Hoesen et al., 1993), area 24b, is more influenced by TUS to the ACC target region. (d) Analysis of the dynamic range of the BOLD signal across all voxels in (i) the control state, (ii) after amygdala TUS, and (iii) after ACC TUS revealed similar levels of variance in activity in all three cases.

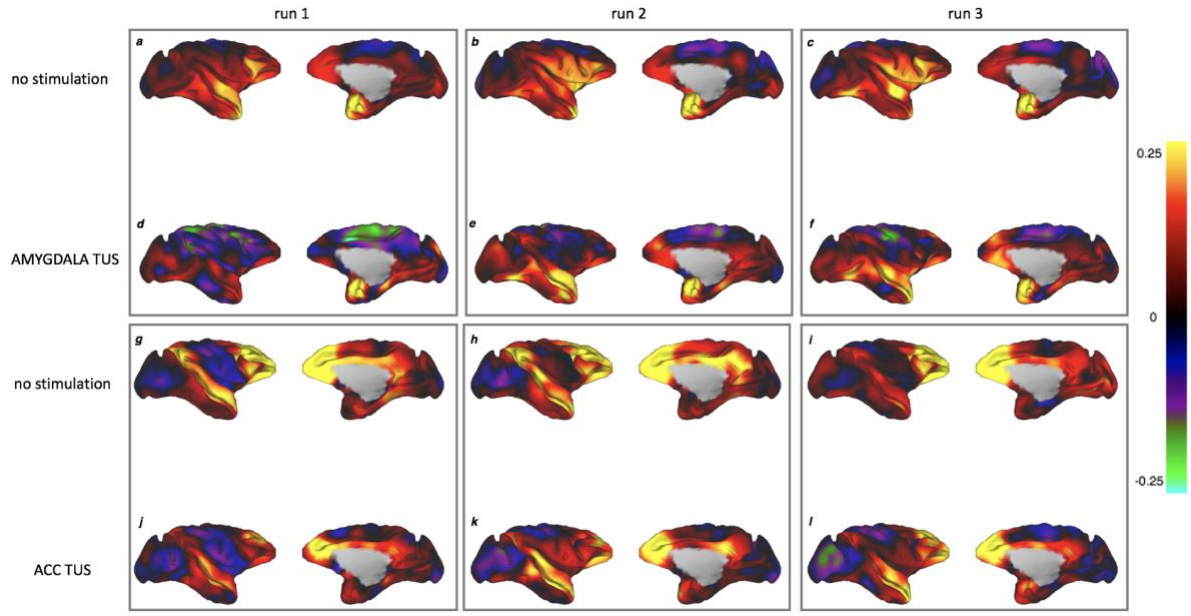

Supplementary figure 3. Temporal changes of TUS effects on amygdala and ACC functional coupling. Amygdala functional coupling (a,b,c) and ACC (d,e,f) functional coupling across 3 consecutive runs is displayed after no stimulation (amygdala: a,b,c; ACC: g,h,i) and TUS (amygdala: d,e,f; ACC: j,k,l). TUS effects on the whole-brain coupling of each stimulated region persisted throughout the full length of scanning. Interestingly, TUS effects seems to show slightly decrease over the three runs with amygdala and ACC functional coupling resembling more their correspondent coupling in the no stimulation condition..

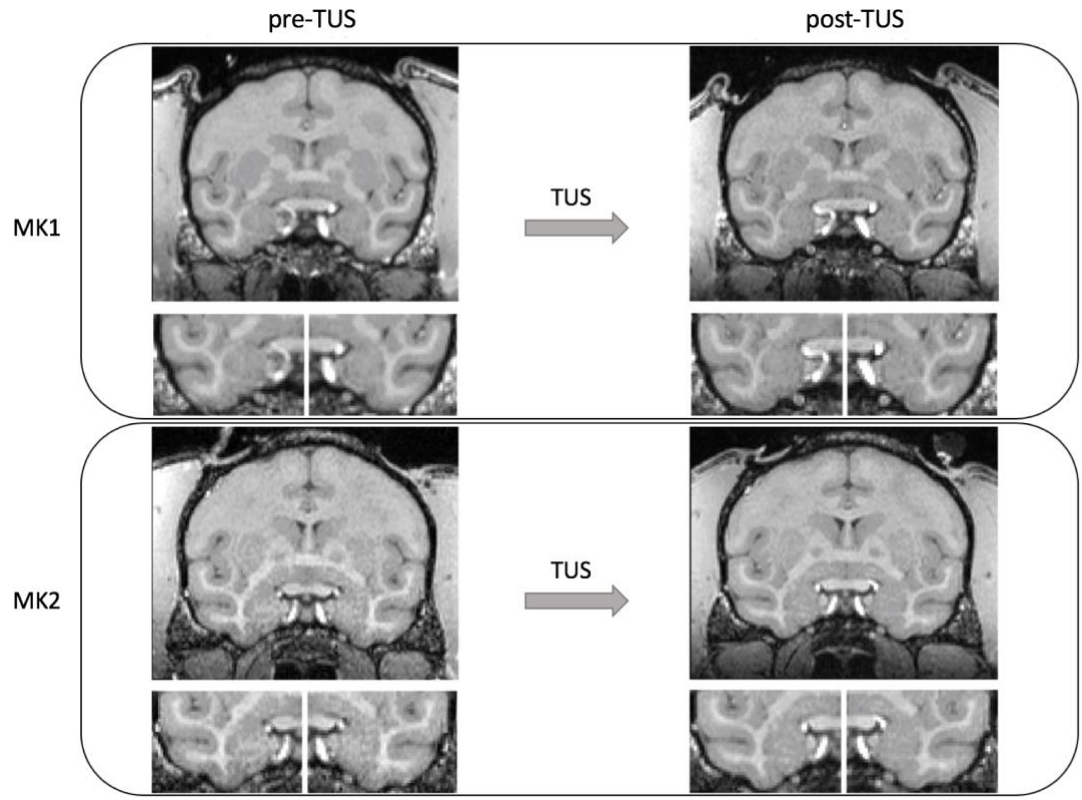

Supplementary Figure 4. Lack of effects of TUS on brain tissue. Coronal T1-weighted images collected before and after TUS (in this example targeted bilaterally to the amygdala) representing the stimulated brain area. Neither structural changes nor evidence of transient edema were found following TUS targeted to the amygdala bilaterally in two exemplar animals.